SAE INTERNATIONAL

ARTICLE INFO

Article ID: 03-13-02-0017

doi:10.4271/03-13-02-0017

Development of a 3D-Computational Fluid Dynamics Model for a Full Optical High-Pressure Dual-Fuel Engine

***Stephanie Frankl*[1] *and Stephan Gleis*[1]**

[1]*Technical University of Munich, Germany*

Abstract

In times of ever stricter exhaust emission regulations, the importance of alternative combustion processes in internal combustion engines continues to grow. One approach to create a combustion progress which produces low CO_2, soot, and methane emissions is the "High-Pressure Dual-Fuel" (HPDF)-combustion. Here, the direct-injected methane is ignited by a small amount of pilot-diesel and burns in a diffusive combustion mode.

This study describes the development of a three-dimensional computational fluid dynamics (3D-CFD) model for the HPDF-combustion. A Reynolds-Averaged Navier-Stokes (RANS) approach with k-epsilon modelling for turbulence was chosen for the calculation of the flow field. The pilot fuel injection is implemented by using Lagrangian Particle Methods, whereas the gas injection is a mass flow boundary which is derived from measurements of the injector. The model is validated using data from a fully optically accessible single-cylinder research engine. The flow field is compared with particle image velocimetry (PIV) data taken before the start of injection (SOI). Concerning pilot injection, a grid convergence study is conducted and an optimization is developed to reduce computational costs. The penetration length of the liquid fuel spray is validated against Mie-scattering images which are taken during the "Pilot-Diesel-only" experiments in the fully optical single-cylinder research engine.

The ignition and combustion is modeled via detailed chemistry, which is solved using the commercial Software CONVERGE and the SAGE chemistry solver. The flame liftoff length of the pilot-diesel and the ignition and combustion of the underexpanded gas jets are validated using high-speed imaging of flame luminosity and OH* chemiluminescence. It can be shown that the used *n*-heptane mechanism is capable of correctly reproducing the trends in the ignition and combustion process.

History

Received: 26 Aug 2019
Revised: 09 Dec 2019
Accepted: 07 Jan 2020
e-Available: 27 Jan 2020

Keywords

Dual-Fuel, Gas-Direct-Injection, Optical-Engine, CFD-Simulation

Citation

Frankl, S. and Gleis, S., "Development of a 3D-Computational Fluid Dynamics Model for a Full Optical High-Pressure Dual-Fuel Engine," *SAE Int. J. Engines* 13(2):241-252, 2020, doi:10.4271/03-13-02-0017.

ISSN: 1946-3936
e-ISSN: 1946-3944

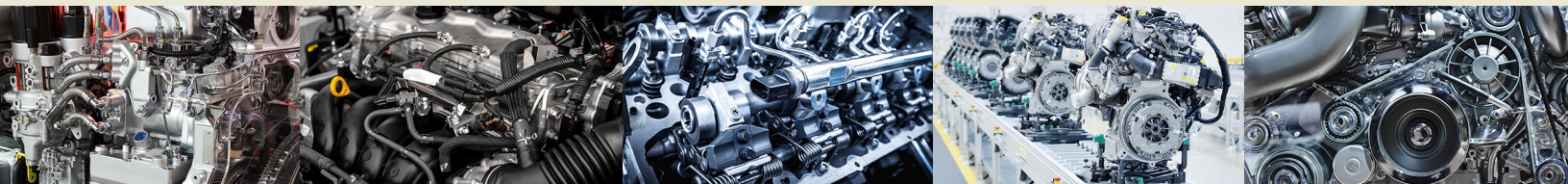

1. Introduction

In the common Dual-Fuel Engine concept, the main fuel is injected into the intake air and ignited by a small amount of diesel at the end of the compression stroke. Due to quenching effects and valve overlap, methane from the gaseous fuel slips into the exhaust gases. Worldwide unburned hydrocarbons (HC) are restricted by laws and international conventions, for example, the MARPOL [1] or the Non-Road Mobile Machinery regulations in the European Union (EU) [2]. Therefore it is a main goal to minimize the HC emissions. One possibility to reach the HC regulations is the high-pressure direct injection of natural gas short before the compression stroke top dead center (TDC) which is ignited by a small amount of pilot-diesel injection, the so-called High-Pressure Dual-Fuel (HPDF)-combustion.

1.1. State of the Art

In the 1990s, P. Oullette studied the high-pressure direct injection of natural gas for diesel engine fueling [3]. He concentrated on the jet penetration and the mixing of the underexpanded gas jets. A rudimental simulation model, developed to investigate the dual-fuel combustion, used the KIVA Code for the 3D simulation. The results were validated against Schlieren images of cold methane gas jets [4]. The intended use was a dual-fuel application for heavy-duty vehicles. On basis of Oullette's work, Westport developed the first dual-fuel injector with concentric needles [5]. From thereon, a lot of experimental work was done to investigate the complex processes of ignition and combustion.

McTaggart-Cowan carried out studies about the influence of the gas injection pressure level and found a significant influence on the emissions [6]. Furthermore he surveyed the particle matter reduction [7], which was followed by Munshi [8] and Faghani [9, 10] through variations of the relative injection timings of the pilot and main fuel.

Barba et al. carried out experimental investigations with various gas pressures on a 2-liter (2l) heavy-duty engine. They found out that higher gas pressures lead to a shorter burning time and thus to increasingly diesel-like heat release rates (HRRs) [11].

One of the first optical measurements of the combustion of a high-pressure gas jet was conducted by Imhof [12]. In this work, a rapid compression-expansion machine (RCEM) with two separate injectors was used to simulate a large-bore marine engine. He found that, in comparison to a diesel engine, the HRR of the diffusive gas combustion is similar, but the NOx and soot emissions are significantly lower [13]. His work was continued by Takasaki [14], who used the same machine to optically investigate methane-hydrogen mixtures.

Also using a RCEM, Fink and Jud investigated the influence of spatial and temporal interaction of a gas jet and the pilot-diesel on ignition and combustion using the shadowgraph technique [15]. They have found out that, at simultaneous injection, if the two fuel jets are arranged approximately parallel, ignition can fail. This occurs because the gas jet sucks up the pilot-diesel so the diesel spray lies within the gas jets and does not mix with air. On the other hand, if the angle between the two fuels is too big, the gas jet does not ignite either because the gas jets do not reach the hot combustion products from the diesel. This data was used by Woodward L'Orange to develop spray targeting for a high-pressure dual-fuel injector [16], which is also used in this study (Figure 1).

From the beginning, most of the mentioned investigations were accompanied by 3D-CFD simulations to facilitate the interpretation of the results (e.g., [17, 18, 19, 20, 21]). They are used to identify ignition locations and sources of emission and particle formation.

There are only a few sources in literature for the application of the combustion process in optically accessible engines. The first one to publish an optical study combined with CFD results was Hatzipanagiotou [22]. He carried out high-speed imaging on a heavy-duty engine using the Westport HPDI injector, comparing the results versus CFD calculations of the same engine. The latest study is from Rochussen, who did OH*-chemiluminescence and Natural Gas luminosity imaging on a 2l Ricardo Proteus engine [23]. Both studied the influence of the relative injection timing of the two fuels on ignition and reaction zone growth.

1.2. Present Work

The state of the art shows that there is a lack of well-validated CFD models for the HPDF-combustion in high-speed medium-sized engines. So in this work a multidimensional model of the experimental fully optically single-cylinder engine is built up and validated against the measured data and the high-speed imaging. This includes validation of the flow field with PIV as well as liquid penetration length of the pilot-diesel with Mie scattering. The flame liftoff length is compared to the high-speed flame luminosity images and

FIGURE 1 Nozzle with three concentric gas needles and one central diesel needle of the Woodward L'Orange HPDF-Injector.

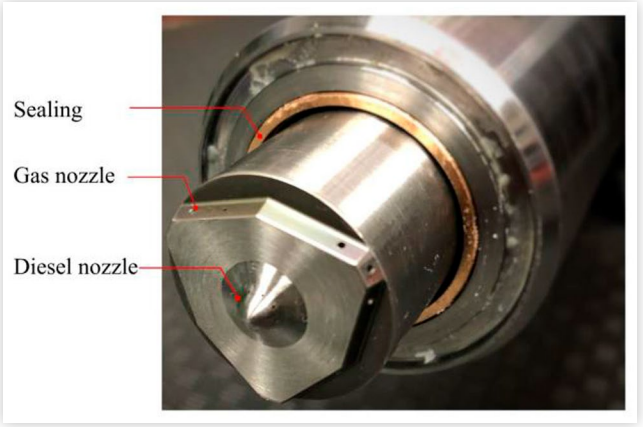

OH*-chemiluminescence shots. Afterwards further progression of the underexpanded gas jet is investigated in detail.

2. Methodology

2.1. Experimental Setup

2.1.1. Engine Parameters The test rig used for the experimental surveys is a fully optically accessible single-cylinder engine equipped with the HPDF-Injector from Woodward L'Orange, as shown in Figure 1. The injector uses a 3-1-needle design. There are three concentrically arranged gas needles, where each opens three gas holes. In the middle of the nozzle sits one diesel needle which controls nine holes for the pilot injection. The spray targeting is shown in Figure 2.

The engine has a large bore of 170 and 210 mm stroke. Further data is given in Table 1. The optical accesses of the engine are realized in the "Bowditch Design" [24]. It consists of an elongated piston and an additional lateral access, as shown in Figure 4. A detailed description of the structure can be found in [25, 26, 27, 28].

For the HPDF-combustion experiments, the compression ratio is set to 16.5. Two different inlet camshafts were used to investigate different swirl levels. Figure 3 displays the resulting valve lift curves, one optimized for a maximum fresh air charge and the other with a moderate Miller [29] timing.

The inlet and outlet channels are indicated by pressure sensors as well as temperature sensors. The combustion chamber pressure is measured in 0.1°CA increments.

2.1.2. Optical Setup To validate the flow field PIV images are taken 10°CA ATDC. The test rig is equipped with a Litron Nano TI 200-15-PIV laser for this purpose. The laser sheet is located 15 mm below the fire deck. For seeding particles titanium dioxide is used. Further details can be found in Gleis et al. [27].

The engine is able to take combined high-speed Mie-scattering and flame luminosity images. For the Mie-scattering images, there is a LED flash lamp at the lateral access beneath the cylinder head (see Figure 4). The used high-speed camera takes the images crank angle synchronous in 0.2°CA resolution through the glass insert in the optical piston.

In order to investigate the diesel ignition more closely, OH-chemiluminescence images were also taken. For these, the same high-speed camera with an additional image intensifier of 222 nm wavelength was used.

For the injection a high-pressure dual-fuel injector was used [16]. The nine gas jets are arranged in triplets around a regular nine-hole diesel injector. This design is enabled using three concentric gas needles and one central diesel needle. The experiments are performed with diesel as pilot fuel and

TABLE 1 Engine data.

Displacement	4.77 l
Stroke 2r	210 mm
Bore d	170 mm
Connecting rod length l	480 mm
Compression ratio ε	16.5:1
Number of valves	4
Exhaust valve open	136.5°CA
Exhaust valve close	357°CA
Inlet valve open	341.2°CA
Inlet valve close	562°CA

FIGURE 2 Spray targeting of the HPDF-Injector.

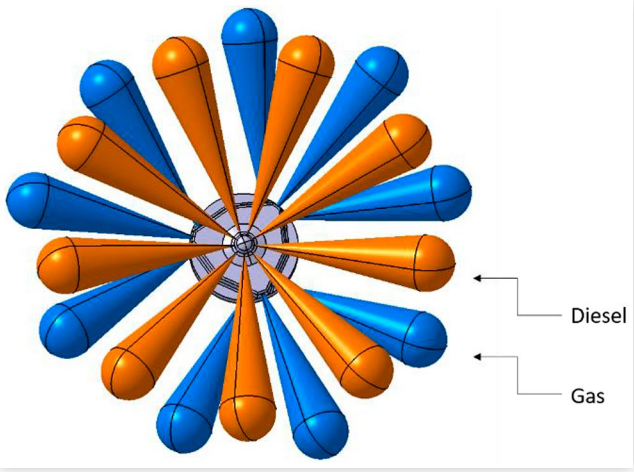

FIGURE 3 Valve lift curves.

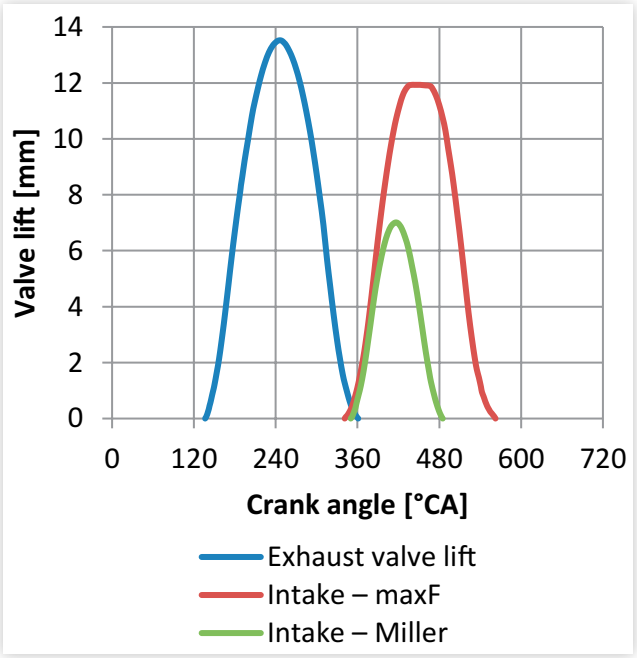

FIGURE 4 Schematic representation of the optical single-cylinder engine.

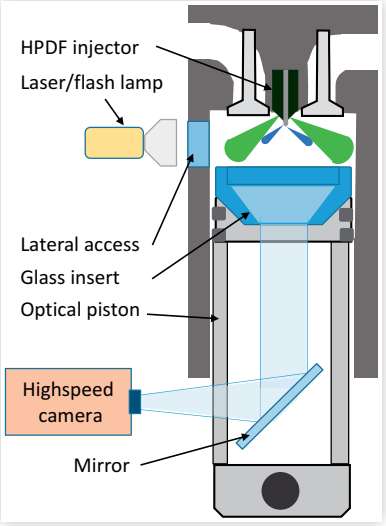

methane as main gaseous fuel. Due to the optical construction, the only cooling for the upper part of the piston is through air ventilation. In order not to overheat the construction, and prevent severe damage, the experiments are conducted in skip fire mode. This means there are 50 fired cycles followed by drag operation to cool down the glass inserts.

2.1.3. Reference Point for Dual-Fuel Operation

The reference point for the dual-fuel operation was chosen at an engine speed of 750 RPM with 2.3 bar inlet pressure. The exhaust pressure is kept at the same value for a better estimation of the charge air per cycle, which is measured via a Coriolis flow meter. The intake air is conditioned to a constant temperature of 318 K.

To avoid severe damage of the optical setup through large pressure gradients, the gas injection takes place short after the piston reaches TDC. The start of energizing (SOE) of the pilot-diesel results from the ignition delay of the diesel; it is chosen in a way that the propagating gas jets hit the igniting diesel cones so the diffusive combustion mode is dominating the combustion of the methane. Table 2 gives the resulting values as well as the injected masses and the injection pressures. The fuel ratio is chosen in a way that the pilot fuel is 10% of the whole energy content. These settings reach an indicated effective mean pressure of 12 bar.

TABLE 2 Injection parameters.

SOE pilot-diesel	−2°CA
SOE gas main injection	−5°CA
m_diesel	31 mg
m_gas	320 mg
p_diesel	1000 bar
p_gas	300 bar

2.2. Numerical Setup

For the 3D-CFD simulations of the described experimental setup, the commercial software package CONVERGE CFD is used. The Reynolds-averaged Navier-Stokes (RANS) equations including the k-epsilon-RNG turbulence model [30] describe the flow field of the gas-exchange cycle and combustion simulations. The "pressure implicit with splitting of operator" (PISO) algorithm from Issa [31] is used to solve the time dependent fluid flow equations. The Peng-Robinson model represents the real gas behavior [32] of the gas phase. The combustion is modelled via the detailed chemistry solver SAGE [33]. In order to keep the computational cost low, the HC mixture diesel is substituted by *n*-heptane in the simulations. *n*-Heptane is often used as reference fuel for diesel for it has a similar LHV of 44.7 MJ/kg [34] and cetane number of approximately 56 [35].

The kinetics is described by the reduced Chalmers 53 *n*-heptane mechanism, which was validated for use for dual-fuel combustion by Jud in [36, 37]. Since methane is an intermediate product of *n*-heptane combustion, reactions for the oxidation of methane are contained in this mechanism.

2.2.1. Charge Exchange Simulation

The chosen domain for the gas-exchange simulation includes the plenum and ends at the beginning of the exhaust system, as shown in Figure 5. Due to the optical engine's design, the crevice volume is increased compared to the all metal engine. It would be too complex to consider them in detail, so they are collected and represented in an extended piston junk volume to retain the correct compression ratio. It is assumed that the flow within the crevices has very low influence on the charge movement [38]. Since this is a direct injection of the gas, there are no unburned HC emissions from crevices as in premixed configurations expected [39].

The experimental pressure measurements are used for the inlet and exhaust boundaries, as well as for initial conditions to reach maximum consistency with experiments. The motion of the piston results from the experimental pressure curves, and the following presumption of the optical piston

FIGURE 5 Domain for charge-exchange simulations.

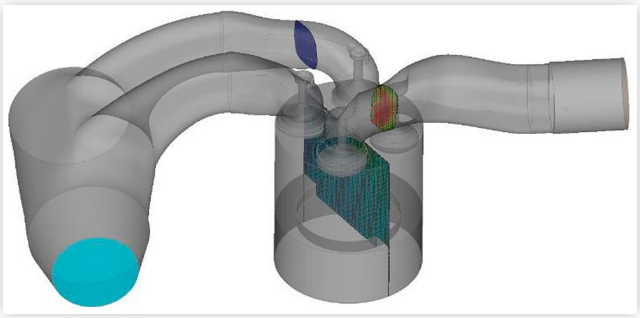

and connecting rod deformation is taken into account. With the deformation

$$\frac{dz}{dp} = 0.7\ \frac{\mu m}{bar} \qquad \text{Eq. (1)}$$

the piston motion results in the equation:

$$s(\varphi,p) = -\frac{dz}{dp} + r\left[1-\cos(\varphi) + \frac{r}{4l}\left(1-\cos(2\varphi)\right)\right] \qquad \text{Eq. (2)}$$

The deformation is a result from a finite elements simulation of the optical piston. CONVERGE uses an orthogonal grid for the discretization of the computational domain [40]. The Base Size of the mesh is 4 mm, with several fixed embedding (FE) refinements, as listed in Table 3. In addition an adaptive mesh refinement (AMR) is in use for the whole domain except the plenum, exhaust, and crevice regions while valves are open. FE and AMR refine or coarsen the grid with embedding scales as follows [40]:

$$\text{Scaled grid size} = \frac{\text{Base size}}{2^{\text{embed. scale}}} \qquad \text{Eq. (3)}$$

Due to the optical engine's lateral access, the temperature wall boundary for the liner is not uniform. The glass heats up to higher temperatures than the steel liner. This is taken into account through a locally defined temperature profile which is 600 K in the area of the lateral glass access and 420 K on the rest of the liner surface. All other walls are assumed to have constant temperature values.

For a reliable result, three consecutive gas exchange cycles are calculated. The initialization of the combustion simulation uses the results from the third cycle.

2.2.2. Pilot-Diesel Simulation Due to the symmetry of the used dual-fuel injector-regular nine-hole diesel injector (see Figure 2), the tuning of the diesel injection parameters is made on a 40° sector mesh. It is initialized by the result of the gas-exchange cycle simulation 10°CA before SOI. The combustion chamber pressure is 36 bar and 850 K of temperature. The diesel injection pressure is 1000 bar, the fuel temperature 350 K, and the injected mass 3.69 mg.

TABLE 3 Fixed embeddings.

Name	FE scale
Crevice	2
Inlet ports	2
Receiver	1
Cylinder	1
Valve seats	3

The diesel injection uses the Lagrangian droplets method to simulate the fluid phase of the fuel with the O'Rourke model for turbulent dispersion and Frossling model for evaporation [40]. The Kelvin-Helmholtz-Aerodynamic Cavitation Turbulence [41] breakup model describes the primary breakup whereas the Rayleigh-Taylor breakup model is used for secondary spray breakup [33, 40]. The discharge coefficient for the nozzle is set to 0.8. Droplet collision is modelled via NTC collision model [42]. The liquid fuel is modelled using the default fuel "DIESEL2" from Converge CFD, which evaporates to n-heptane in gas phase. The injection rate derives from measurements of the injector in an injection rate analyzer. A mesh study based on the results of Senecal et al. [43] was made to determine the values for the mesh size. For this mesh study only the diesel injection was of interest, so it was made on a 40° sector mesh without the sac hole of the gas injector (Section 2.2.3). The determined mesh sizes and related parcel numbers are given in Table 4. The meshes 1-4 and parcel numbers are analog to the study of Senecal et al., but using the geometry of the optical engine and validated with the experimental Mie-scattering images of the liquid diesel phase.

Figure 6 shows the resulting penetration length of the mesh study. Mesh 1 has a too-low rise in the beginning of the injection. The Parcels enter the domain to slow, and the injection does not reach a constant behavior. Meshes 2 and 3 overestimate the penetration length around 714.5°CA by ca. 45% and 18%, whereas they show least deviation while the injection rate is constant.

Mesh 4 shows the best accordance to the measured penetration length in the experiment. The peaks in the penetration length, as in meshes 2 and 3, are eliminated and the constant value of the penetration length has a maximum deviation of 10% from the measurements. Mesh 4 had the highest computational time. To decrease the calculation time, in mesh 5, the parcel number of mesh 3 was used. This divided the calculation time by half, it still avoids the overshoot in the penetration length, but in the constant part of the injection, the penetration deviates 14.3% from the experiment.

A further reduction of the parcel number in mesh 6 led to even shorter calculation times. The maximal deviation results then in 25.6%, and the mean deviation is about 17.5%. This inaccuracy was tolerated for the fact that the computational times could be reduced further to a tenth of mesh 4.

The final mesh for the diesel injection has a two-step cone-shaped embedding for each nozzle. The embedded

TABLE 4 Resulting minimum cell sizes and used parcel numbers of the mesh study.

	Min. cell size	Number of parcels
Mesh 1	0.5	128,000
Mesh 2	0.25	512,000
Mesh 3	0.125	2,048,000
Mesh 4	0.0625	8,192,000
Mesh 5	0.0625	2,048,000
Mesh 6	0.0625	64,000

FIGURE 6 Comparison of the influence of mesh size and parcel number on spray penetration.

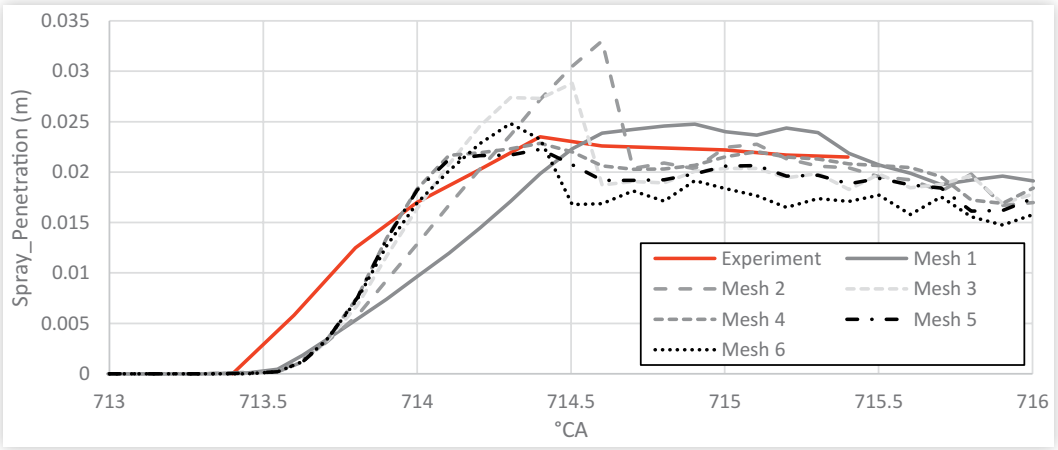

regions overlap and can be seen in Figure 7. The inner cone is a scale 4 embedding, which results in a minimum cell size of 0.0625 mm, and its length is 10 mm. The outer cone is a scale 3 embedding of 25 mm length.

2.2.3. Gas Main Injection The simulations for the gas injection and the dual-fuel combustion is made on 120° sector meshes, as shown in Figure 8.

The gas injection takes part via a mass flow boundary at the cross section 1 mm above of the gas needle seat. The mass flow rate for the gas derives from flow measurement in an IAV Injection Analyzer Gas using nitrogen as medium, which is translated to the characteristics of methane. Because of vorticity effects in the sac hole, it is necessary to lay the boundary short above the seat of the gas needle, as shown in Figure 9.

For the gas injector, a FE scale 3 refines the cells within the sac hole and the nozzle holes. The gas jet itself is refined via temperature and velocity of AMR scale 3 as well. The gas needle of the injector is permanently open for the whole simulation - without any movement. The seat of the gas needle divides the domain into two separate regions, which are connected at the moment when the gas injection starts.

FIGURE 7 Mesh refinements for the liquid diesel injection.

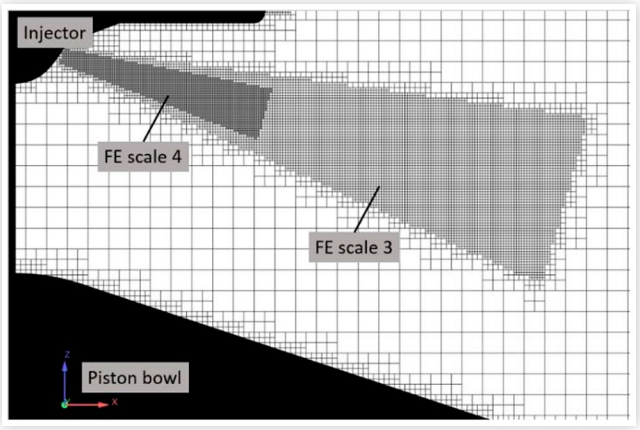

3. Results and Discussion

3.1. Results of the Charge Exchange Simulations

The mesh parameters for the gas exchange simulation were optimized for the reference point. Afterwards it was used for cold flow simulations of different charging air

FIGURE 8 Simulation domain for gas injection and dual-fuel combustion.

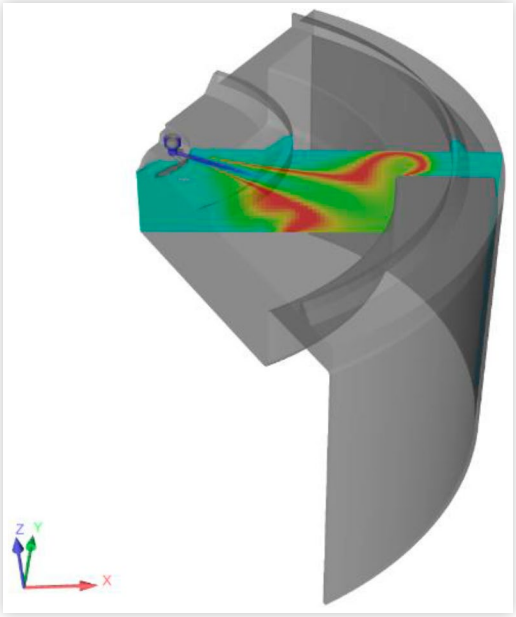

FIGURE 9 Mesh while gas injection is active. Due to vorticity effects the sac hole of the gas injector has to be integrated into the domain.

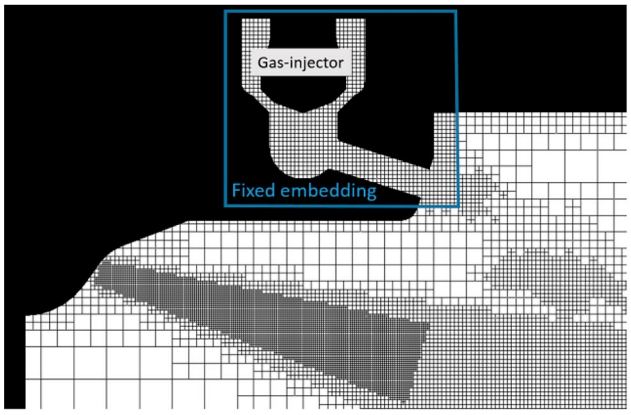

FIGURE 10 Pressure curves of simulation (dots) and experiment (line) for the reference case (Sn256) and a comparison case with different valve timings (Sn1739).

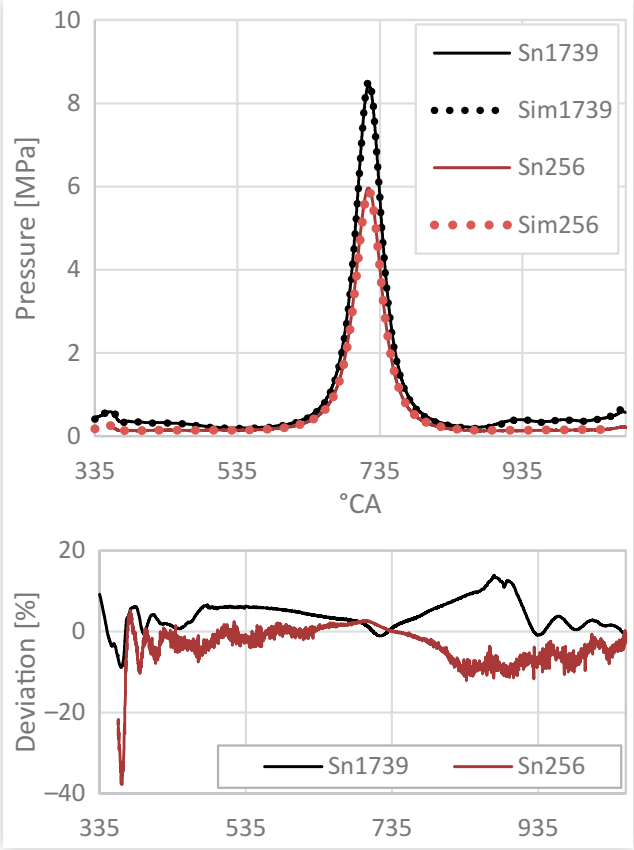

pressures, rotational speed, and valve timings. Comparisons with the measured pressure curves (average of 50 curves) show a very good agreement within plus-minus 10% deviation from the pressure, as in Figure 10. The only exception is at the charge exchange TDC where the reference point has a deviation of 37% for a few crank angles, which is 0.6 bar. The measurement accuracy of the pressure sensor is ±0.2 bar. Therefore, the deviation probably results from the incorrect represented crevice volumes. The deviation from the measured curves is at minimum around the firing TDC, which is ca. 1 bar.

To determine the influence of the fluid flow in the cylinder bowl on the combustion, the fluid flow around the TDC firing is validated against the PIV measurements, as shown in Figure 11. The simulation results show good agreement with the measured data. The absolute values of the velocity are of the same range, and the center of the swirl is dislocated relative to the cylinder axis and rotating.

A closer look at the fluid flow at 710°CA shows that the flow evens as the pistons approach the TDC. The swirl axis lies almost in the center of the cylinder; therefore, the 40° for the diesel combustion and the 120° symmetry for the gas-diesel combustion simulations are justified.

3.2. Results of the Combustion Simulations

3.2.1. Diesel Combustion To validate the combustion simulation, the results of the combustion simulation are compared against the pressure measurements of the experiments. Afterwards they are overlaid with the images of the high-speed cameras. To validate the diesel ignition, the OH-isosurfaces are compared to the OH*-chemiluminescence images. The comparison uses an average of images of 50 cycles at every crank angle to get a valuable result to compare to the simulation.

The result shows a good agreement of the simulated OH with the local distribution of the OH* in the experiment. The ignition, as can be seen in Figure 12 at 715.8°CA, starts at the flanks of the diesel spray cones and spreads to the head of the jet at 717.4°CA. When the combustion continues, the OH region broadens, as it does in the experiment. The flames in combustion and in simulation simultaneously reach the piston bowl wall, which is another sign for the good quality of the CFD model.

Due to the fact that the OH*-chemiluminescence imaging technology produces integral images of the natural activated OH*, which does not equal the full quantity of OH in the simulation [44], no quantitative comparison is possible.

3.2.2. Dual-Fuel Combustion For the Dual-Fuel Combustion, the resulting pressure curves in the cylinder are compared with the measured pressures in the experiment. Furthermore the HRRs from pressure rate analysis are compared with the heat release from the simulation to get a better understanding of the quality of the CFD model (Figure 13).

For the pilot-diesel combustion, the resulting in-cylinder pressure of the simulation is close to the measured pressure in the combustion chamber. At the beginning of the gas

FIGURE 11 Comparison of the PIV measurements (right) and the simulation (left) for the maxF (upper)- and Miller(lower)-valve timing at 710°CA 15 mm below the fire deck.

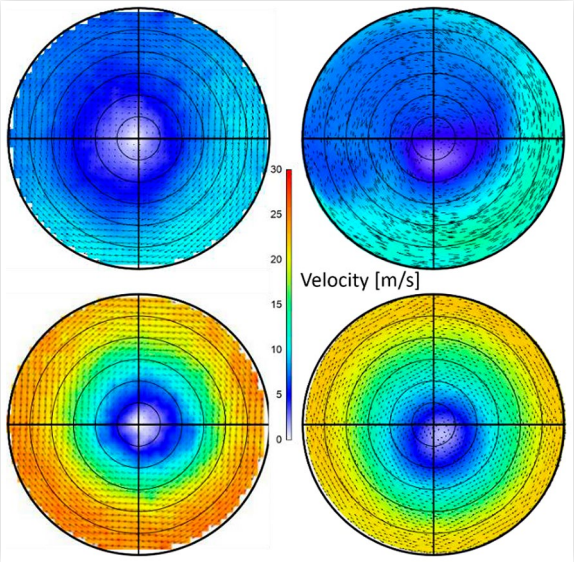

injection, the pressure in the simulation is just 1 bar above the experiment. This is a result of the slightly higher HRR.

The maximum pressure in the experiment is 134 bar at 729°CA whereas the simulation reaches almost the same value of 134 bar, but at 734°CA. With a look at the HRR, it can be seen that the gas in the simulation starts to release heat at the same time as in the experiment, but the peaks are about 250 J/s lower. This changes from 730° to 737°CA; the heat release in the simulation is higher, so the pressure rises above the measured values. From 750°CA the simulated HRR value falls below that from the experiment.

FIGURE 12 Comparison of the OH*-chemiluminescence images and the isosurface of mass fraction of OH (blue) from the CFD results at the beginning of the pilot-diesel ignition.

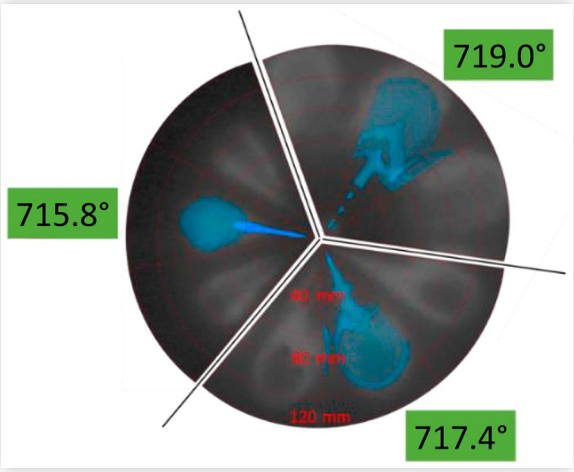

For further insight into the HPDF-combustion, isosurfaces of methane and temperature are compared with the high-speed images. The temperature isosurfaces value is 1500 K for the fact that soot luminosity is within the visible range above this temperature. The methane isosurface lies at 0.02% mass fraction.

Figure 14 shows the overlaid pictures from the experiment (background) and simulation. At 721.6°CA the pilot-diesel ignites and the gas injection starts. There is also a small amount of methane visible within the diesel combustion, for the fact that CH_4 is produced as decomposition product of the heptane combustion. In the next step shown at 723.2°CA, the gas injection has started to expand. It can be detected in the experiment as the small bright areas between the burning diesel cones. In the simulation the methane injection can be observed via the three blue cones emerging from the gas injector holes.

As the gas further emerges into the combustion chamber, it can be seen that the penetration length fits quite good. When the tips of the gas jets shoot past the burning diesel, parts of the

FIGURE 13 Comparison of simulation (red line) and experiment (gray); measured pressure curves and derived HRRs.

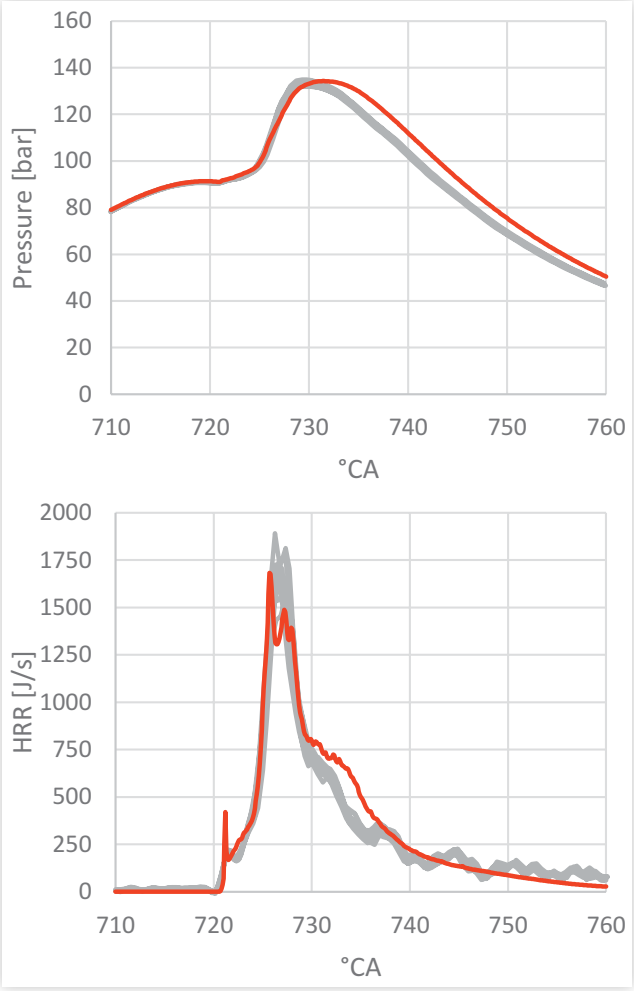

FIGURE 14 Comparison of simulation isosurfaces (orange T = 1500 K, blue CH_4 = 2%) and experiment (gray, background).

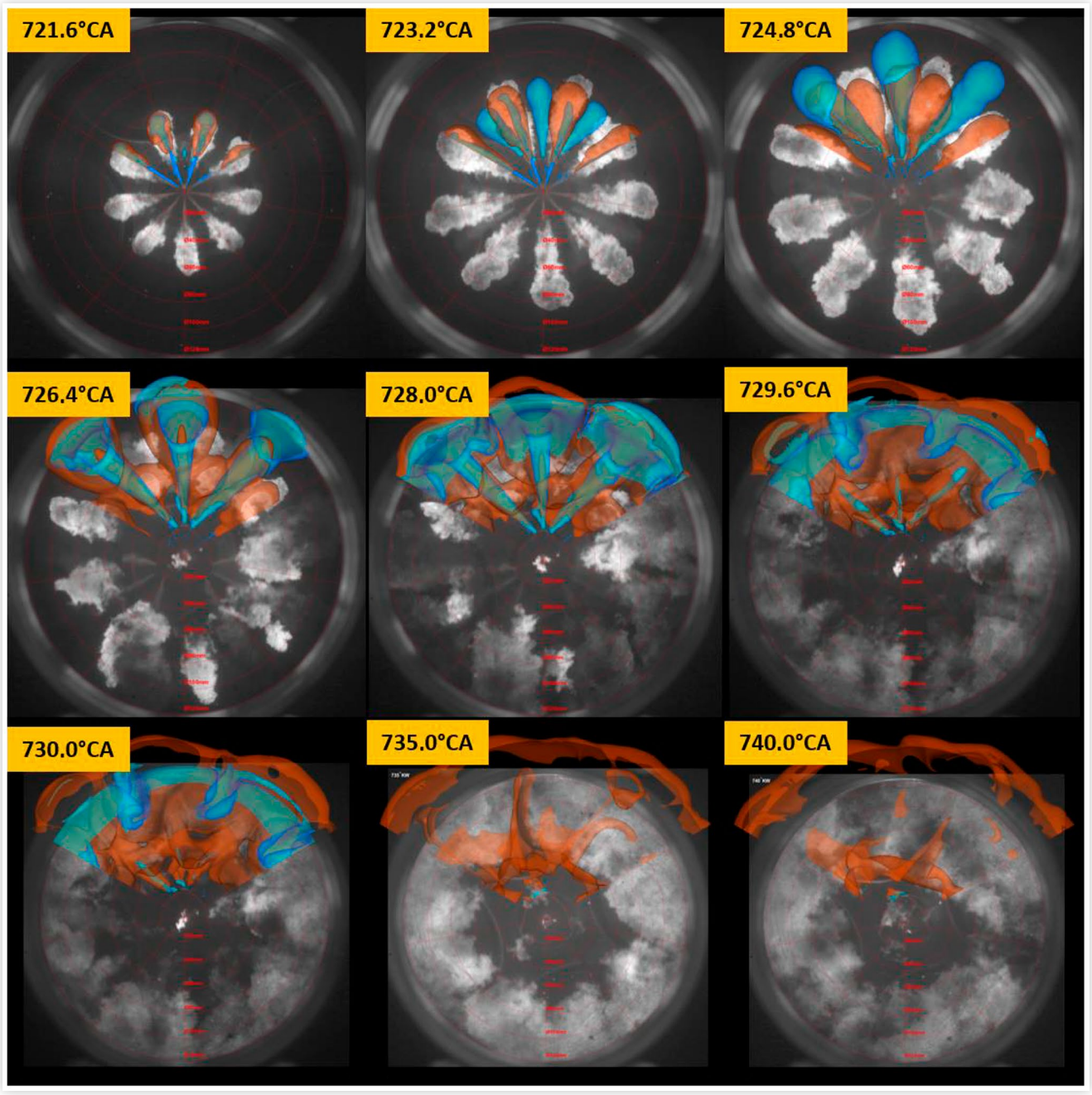

hot combustion gases are entrained. In the experiment this can only be guessed by the blurriness of the diesel luminosity (724.8°CA) - which does not happen in the diesel-only pictures. In the simulation, on the other hand, it can be clearly seen that the temperature isosurfaces extend into the gas jets. In the following pictures it can be seen that the methane ignites from behind. The gas jets reach the piston bowl walls before igniting completely. Therefore, they form a very rich mixture at the piston bowl walls. This is accompanied by soot illumination in the gas combustion (726.4°-729.6°CA) and the high values in the HRR in Figure 13. In the lower part of Figure 14, it can be seen that there is a big amount of CH_4 at the piston bowl wall which vanishes until 735°CA. In the experiment the soot illumination from the gas combustion intensifies and slows down again until 740°CA, where most of the combustion is over.

3.3. Discussion of the Results

The charge exchange shows good agreement to the measurements. This was achieved by a modified stroke, temporal wall boundary for the liner, and an additional crevice volume for

the optical accesses. For the mesh FEs on the boundaries and AMR are used. There is a chance that the experiment is influenced by blow-by rates. The engine is equipped with PTFE piston rings which last about three hours of operation until they get worn and the blow-by rises. For comparison with the CFD results, the experiments taken short after changing the rings are preferred to minimize the influence of blow-by. Nevertheless, the measured and the simulated velocity fields 15 mm below the cylinder deck show a good agreement for both of the considered points. The velocity magnitudes are of the same range, and the areas of higher and lower gas motion are represented well in the simulation.

Simulating the pilot-diesel, it is obvious that the initial spray penetration length in the simulation is always underestimated compared to the Mie-scatter imaging. One reason for this could be inaccuracies in the measured injection rate. Improvement of this will be part of future optimization of the model. In order to optimize the computing time, the number of particles was reduced while the cell size was kept at constant values. A mean deviation of 17.5% in the liquid penetration length was accepted in order to reduce the calculation time by factor 10. The location and timing of the pilot ignition are still in good agreement with the experimental recordings, which enable a locally correct ignition source for the main gas fuel.

The gas combustion also shows good agreement with the measured values. The ignition delay of the methane ignition fits the experiments quite well. The increase in the HRR is steeper in the simulation than in the experiment. One reason for this could be that in the experiment not all gas needles open exactly the same (within microseconds) and therefore a small part of the fuel gas ignites later, whereas in the simulation, due to the symmetry boundaries, the injections are assumed identical.

3.4. Conclusion and Outlook

In this work a simulation model for the high-pressure dual-fuel combustion was developed and validated.

To properly simulate the liquid phase of the diesel injection a mesh study was conducted. The final computational mesh consists of a combination of FEs and AMR.

In order to realize the gas injection, the lowest part of the nozzle geometry is included in the simulation to avoid a supercritical boundary condition at the gas inlet.

The results of the dual-fuel injection show good agreement with the high-speed flame luminosity images.

Further development of the model is still necessary, to better match the liquid spray penetration length of the diesel injection and the HRRs of the experiments.

The knowledge of the actual wall temperatures has to be optimized. Therefore the engine will be equipped with additional thermocouples in the cylinder head and at the optical accesses in the future.

Furthermore the simulation model has to be tested against various speeds and loads. In order to simulate real gas qualities with amounts of propane and ethane, it could be necessary to include additional reactions and species to the used reaction mechanism.

As shown in the Section 1.1, for marine high-speed engines these are one of the first researches which was done in this engine size and displacement with high-pressure gas direct injection and diffusive combustion.

Abbreviations

AMR - Adaptive mesh refinement

CA - Crank angle

FE - Fixed embedding

HPDF - High-pressure dual-fuel

SOE - Start of energizing

SOI - Start of injection

TDC - Top dead center

References

1. International Maritime Organization, MARPOL: Consolidated Edition, 2011; Articles, Protocols, Annexes and Unified Interpretations of the International Convention for the Prevention of Pollution from Ships, 1973, as Modified by the 1978 and 1997 Protocols, Fifth edition. London: International Maritime Organization, 2011.
2. Parliament Office, "REGULATION (EU) 2016/ 1628 OF THE EUROPEAN PARLIAMENT AND OF THE COUNCIL - of 14 September 2016 - On Requirements Relating to Gaseous and Particulate Pollutant Emission Limits and Type-Approval for Internal Combustion Engines for Non-Road Mobile Machinery, Amending Regulations (EU) No. 1024/2012 and (EU) No. 167/2013, and Amending and Repealing Directive 97/68/EC: EU 2016/1628," *Official Journal of the European Union*, 2016, 53-117.
3. Oullette, P., "Direct Injection of Natural Gas for Diesel Engine Fueling: A Thesis submitted in partial fulfillment of the requirements for the degree of doctor of philosophy," Dissertation, Department of Mechanical Engineering, University of British Columbia, Vancouver, 1996.
4. Hill, P.G. and Ouellette, P., "Transient Turbulent Gaseous Fuel Jets for Diesel Engines," *J. Fluids Eng.* 121(1):93, 1999.
5. Westport, "HPDI 2.0 Injector," http://www.westport.com/is/core-technologies/hpdi-2#what-is-hpdi-2.0, accessed December 13, 2017.
6. McTaggart-Cowan, G.P. et al., "The Effects of High-Pressure Injection on a Compression-Ignition, Direct Injection of Natural Gas Engine," *J. Eng. Gas Turbines Power* 129(2):579, 2007.
7. McTaggart-Cowan G.P., Mann K., Huang J., Wu N. et al., "Particulate Matter Reduction from a Pilot-Ignited, Direct Injection of Natural Gas Engine," in *Proceedings of the ASME 2012 Internal Combustion Engine Division Fall Technical Conference*, Vancouver, 2012, 427.

8. Munshi S.R., McTaggart-Cowan G.P., Huang J., and Hill P.G., "Development of a Partially-Premixed Combustion Strategy for a Low-Emission, Direct Injection High Efficiency Natural Gas Engine," in *Proceedings of the ASME 2011 Internal Combustion Engine Division Fall Technical Conference*, Detroit, 2011, 515-528.
9. Faghani, E., Kheirkhah, P., Mabson, C., McTaggart-Cowan, G. et al., "Effect of Injection Strategies on Emissions from a Pilot-Ignited Direct-Injection Natural-Gas Engine - Part I: Late Post Injection," SAE Technical Paper 2017-01-0774, 2017, https://doi.org/10.4271/2017-01-0774.
10. Faghani, E., Kheirkhah, P., Mabson, C., McTaggart-Cowan, G. et al., "Effect of Injection Strategies on Emissions from a Pilot-Ignited Direct-Injection Natural-Gas Engine - Part II: Slightly Premixed Combustion," SAE Technical Paper 2017-01-0763, 2017, https://doi.org/10.4271/2017-01-0763.
11. Barba, C., Dyckmans, J., Förster, J., and Schnekenburger, T., "Natural Gas-Diesel Dual Fuel for Commercial Vehicle Engines," in *Internationaler Motorenkongress 2017*, Baden-Baden, Germany, 2017, 391-407.
12. Imhof, D., "Visual Combustion Studies for Environmentally Friendly Marine Diesel and Gas Engines," Dissertation, Laboratory of Energy and Combustion (ECO), Kyushu University, Japan, Kyushu, 2013.
13. Imhof, D., Tsuru, D., Tajima, H., and Takasaki, K., "High-Pressure Natural Gas Injection (GI) Marine Engine Research with a Rapid Compression Expansion Machine," in *13. CIMAC*, Shanghai, 2013.
14. Takasaki, K., Tsuru, D., Ueno, R., Asano, S. et al., "Visual Study on GI (Gas High-Pressure Injection) Combustion for Highly Efficient Gas Engine," in *15th Conference "The Working Process of the Internal Combustion Engine"*, Graz, 2015, 403-415.
15. Fink, G., Jud, M., and Sattelmayer, T., "Influence of the Spatial and Temporal Interaction Between Diesel Pilot and Directly Injected Natural Gas Jet on Ignition and Combustion Characteristics," *J. Eng. Gas Turbines Power* 140(10):102811, 2018.
16. Senghaas, C., Willmann, M., and Berger, I., "New Injector Family for High Pressure Gas and Low Caloric Liquid Fuels," in *29th CIMAC Congress*, Vancouver, 2019.
17. Keskinen, K., "Numerical Studies for Charge Formation in Combustion Engines," Dissertation, Department of Mechanical Engineering, Thermodynamics and Combustion Technology, Aalto University, Aalto, Finland, 2018.
18. Choi, M., Lee, S., and Park, S., "Numerical and Experimental Study of Gaseous Fuel Injection for CNG Direct Injection," *Fuel* 140:693-700, 2015.
19. Hamzehloo, A. and Aleiferis, P.G., "Numerical Modelling of Transient Under-Expanded Jets under Different Ambient Thermodynamic Conditions with Adaptive Mesh Refinement," *International Journal of Heat and Fluid Flow* 61:711-729, 2016.
20. Li, M., Zhang, Q., Li, G., and Li, P., "Effects of Hydrogen Addition on the Performance of a Pilot-Ignition Direct-Injection Natural Gas Engine: A Numerical Study," *Energy Fuels* 31(4):4407-4423, 2017.
21. Huang J., McTaggart-Cowan G., and Munshi S., "Large-Eddy Simulation of Direct Injection Natural Gas Combustion in a Heavy-Duty Truck Engine Using Modified Conditional Moment Closure Model with Low-Dimensional Manifold Method," *International Journal of Engine Research*, 1-14, 146808741878285, 2018.
22. Hatzipanagiotou A. et al., "Numerische und optische Analyse der Gas-Diffusionsverbrennung mit Diesel-Pilotzündung in NFZ-Motoren," *International Journal of Engine Research*, 109-119, 146808741773891, 2017.
23. Rochussen, J., McTaggart-Cowan, G., and Kirchen, P., "Parametric Study of Pilot-Ignited Direct-Injection Natural Gas Combustion in an Optically Accessible Heavy-Duty Engine," *International Journal of Engine Research* 121:1-17, 2019.
24. Bowditch, F.W., "A New Tool for Combustion Research A Quartz Piston Engine," SAE Technical Paper 610002, 1961, https://doi.org/10.4271/610002.
25. Korb B., Prager M., and Wachtmeister G., "Ursachen und Reduzierung der CH4-Emissionen in Biogasmotoren; Teilvorhaben 1: Abschlussbericht zum Forschungsprojekt," Technische Universität München, Jan. 2016.
26. Frankl S., Gleis S., and Wachtmeister G., "Interpretation of Ignition and Combustion in a Full-Optical High-Pressure-Dual-Fuel (HPDF) Engine Using 3D-CFD Methods," in *29th CIMAC Congress*, Vancouver, 2019.
27. Gleis, S., Frankl, S., Waligorski, D., Prager, M. et al., "Investigation of the High-Pressure-Dual-Fuel (HPDF) Combustion Process of Natural Gas on a Fully Optically Accessible Research Engine," SAE Technical Paper 2019-01-2172, 2019, https://doi.org/10.4271/2019-01-2172.
28. Karmann, S.B., Prager, M., and Wachtmeister, G., "Conceptual Investigations on Full Optical Accessibility to Large-Bore Medium-Speed Engines," *SAE Int. J. Engines* 12(3):291-308, 2019, https://doi.org/10.4271/03-12-03-0020.
29. Miller, R., "High-Pressure Supercharging System," U.S. Patent 2670595, Application no. US12216749A, March 2, 1954.
30. Han, Z. and Reitz, R.D., "Turbulence Modeling of Internal Combustion Engines Using RNG k-ε Models," *Combustion Science and Technology* 106(4-6):267-295, 1995.
31. Issa, R.I., "Solution of the Implicitly Discretised Fluid Flow Equations by Operator-Splitting," *Journal of Computational Physics* 62(1):40-65, 1986.
32. Peng, D.-Y. and Robinson, D.B., "A New Two-Constant Equation of State," *Ind. Eng. Chem. Fund.* 15(1):59-64, 1976.
33. Senecal, P., Pomraning, E., Richards, K., Briggs, T. et al., "Multi-Dimensional Modeling of Direct-Injection Diesel Spray Liquid Length and Flame Lift-Off Length Using CFD and Parallel Detailed Chemistry," SAE Technical Paper 2003-01-1043, 2003, https://doi.org/10.4271/2003-01-1043.
34. Tao, F., Reitz, R.D., and Foster, D.E., "Revisit of Diesel Reference Fuel (*n*-Heptane) Mechanism Applied to Multi-Dimensional Engine Simulation," in *Seventeenth International Multidimensional Engine Modeling User's Group Meeting at the SAE Congress*, Detroit, MI, April 15, 2007.

35. Curran, H.J., Gaffuri, P., Pitz, W.J., and Westbrook, C.K., "A Comprehensive Modeling Study of *n*-Heptane Oxidation," *Combustion and Flame* 114(1-2):149-177, 1998.

36. Jud, M., Fink, G., and Sattelmayer, T., "Predicting Ignition and Combustion of a Pilot Ignited Natural Gas Jet Using Numerical Simulation Based on Detailed Chemistry," in *Proceedings of the ASME 2017 Internal Combustion Engine Division Fall Technical Conference*, Seattle, 2017.

37. Jud, M., Wieland, C., Fink, G., and Sattelmayer, T., "Numerical Analysis of the Combustion Process in Dual-Fuel Engines with Direct Injection of Natural Gas," in *Proceedings of the ASME 2018 Internal Combustion Fall Technical Conference*, San Diego, 2018.

38. Stocchi, I., Liu, J., Dumitrescu, C.E., Battistoni, M. et al., "Effect of Piston Crevices on the Numerical Simulation of a Heavy-Duty Diesel Engine Retrofitted to Natural-Gas Spark-Ignition Operation," *Journal of Energy Resources Technology* 141(11):2159, 2019.

39. Ambrogi, L., Liu, J., Battistoni, M., Dumitrescu, C. et al., "CFD Investigation of the Effects of Gas' Methane Number on the Performance of a Heavy-Duty Natural-Gas Spark-Ignition Engine," SAE Technical Paper 2019-24-0008, 2019, https://doi.org/10.4271/2019-24-0008.

40. CONVERGE Manual, "CONVERGE: Convergent Science," 2018.

41. Som, S. and Aggarwal, S.K., "Effects of Primary Breakup Modeling on Spray and Combustion Characteristics of Compression Ignition Engines," *Combustion and Flame* 157(6):1179-1193, 2010.

42. Schmidt, D.P. and Rutland, C.J., "A New Droplet Collision Algorithm," *Journal of Computational Physics* 164(1):62-80, 2000.

43. Senecal, P.K., Pomraning, E., Richards, K.J., and Som, S., "Grid-Convergent Spray Models for Internal Combustion Engine CFD Simulations," in *ASME 2012 Internal Combustion Engine Division Fall Technical Conference*, Vancouver, 2012, vol. 2012, 697.

44. Lauer, M.R.W., "Determination of the Heat Release Distribution in Turbulent Flames by Chemiluminescence Imaging," München, Techn. Univ., Diss., Munich, 2011, 1st ed. München: München; Verl. Dr. Hut, 2011.